DOI: 10.1021/ma900401a

Macromolecules
ARTICLE

Ionic Conductivity of Block Copolymer Electrolytes in the Vicinity of Order−Disorder and Order−Order Transitions

Nisita S. Wanakule,[†] Ashoutosh Panday,[†,‡] Scott A. Mullin,[†,‡] Eliot Gann,[⊥] Alex Hexemer,[⊥] and Nitash P. Balsara*[,†,‡,§]

[†]*Department of Chemical Engineering, University of California, Berkeley, California 94720,* [‡]*Environmental Energy and Technologies Division, Lawrence Berkeley National Laboratory, Berkeley, California 94720,* [§]*Materials Sciences Division, Lawrence Berkeley National Laboratory, Berkeley, California 94720, and* [⊥]*Advanced Light Source, Lawrence Berkeley National Laboratory, Berkeley, California 94720*

Received February 20, 2009; Revised Manuscript Received June 11, 2009

ABSTRACT: Order−order and order−disorder phase transitions in mixtures of poly(styrene-*block*-ethylene oxide) (SEO) copolymers and lithium bis(trifluoromethylsulfonimide) (LiTFSI), a common lithium salt used in polymer electrolytes, were studied using a combination of small-angle X-ray scattering (SAXS), birefringence, and ac impedance spectroscopy. The SEO/LiTFSI mixtures exhibit lamellar, hexagonally packed cylinders, and gyroid microphases. The molecular weight of the blocks and the salt concentration was adjusted to obtain order−order and order−disorder transition temperatures within the available experimental window. The ionic conductivities of the mixtures, normalized by the ionic conductivity of a 20 kg/mol homopolymer PEO sample at the salt concentration and temperature of interest, were independent of temperature, in spite of the presence of the above-mentioned phase transitions.

Introduction

There is a growing interest in the use of microphase-separated block copolymers as electrolytes in batteries and fuel cells.[1−16] In these applications, either block copolymers are mixed with ionic species such as lithium salts blended with poly(ethylene oxide)-containing copolymers or ionic species are incorporated in the block copolymer chain as in the case in poly(styrenesulfonate)-containing block copolymers. Because of the fact that most organic polymers are not compatible with ions, ion transport is usually restricted to one of the microphases of the block copolymer. The use of block copolymers may enable the creation of well-defined, optimized pathways for ion transport. In addition, the chemical composition and morphology of the nonconducting microphase can be tuned to optimize other aspects of the electrolyte such as puncture strength or shear modulus. While the ion-conducting pathways can be aligned by the application of external fields,[17−23] the present paper is concerned with samples with randomly oriented morphologies obtained in the absence of external fields.

Order−disorder transitions (ODTs) in block copolymers have been the subject of extensive studies after the pioneering theoretical work of Leibler.[24] At high temperatures, entropic factors dominate and a disordered phase (DIS) is obtained. Energetic interactions between the blocks dominate at low temperatures, leading to the formation of microphase-separated states. The four kinds of microphase-separated states typically found in diblock copolymer melts are spheres packed on a body centered cubic lattice (BCC), cylinders packed on a hexagonal lattice (HEX), the gyroid phase which is a cubic network morphology (GYR), and lamellae (LAM).[2,24−36] It is reasonable to assume that the conductivity of block copolymers with one ionically conducting block, σ, is proportional to the volume fraction of the conducting block, ϕ_C. For unaligned samples, we also expect the conductivity to depend on the tortuosity of the pathways for ion transport, which we account for by introducing the morphology factor, f. We thus write

$$\sigma = f\phi_C\sigma_C \quad (1)$$

where σ_C is the intrinsic conductivity of the conducting microphase. In the case of randomly oriented lamellar grains, Sax and Ottino[37] argue that, on average, one-third of the grains will contain lamellae oriented perpendicular to the direction of charge transport, implying that $f = 2/3$. Similar arguments lead to an estimate of $f = 1/3$ for a HEX morphology with the conducting phase as the minor component. In the case of the GYR phase, the presence of a three-dimensional network ensures transport in the desired direction is never blocked. We thus expect $f = 1$ in this case. Similarly, if the conducting phase is the major component in either BCC or HEX phases, then we also expect $f = 1$. Our use of eq 1 to study the effect of morphology on conductivity of block copolymer electrolytes is based on two implicit assumptions: (1) the intrinsic conductivity of the conducting phase (σ_C) is not affected by morphology, and (2) barriers to transport occurring at grain boundaries are negligible.

Let us, for the moment, consider the most widely studied block copolymer phase transition, namely the ODT of symmetric copolymers that form LAM in the microphase-separated state. To predict changes in conductivity at the ODT, we need to know if eq 1 is valid for disordered block copolymers. The validity of eq 1 will depend on the detailed structure of the disordered phase. There are at least three different senarios. (1) If the disordered phase contains large-amplitude concentration fluctuations, i.e., the sample contains disordered regions of essentially pure conducting and nonconducting phases, and if these regions are cocontinuous, then one might expect eq 1 to be valid with $f = 1$, since there are no blocked transport directions in this system.

*To whom correspondence should be addressed.

 Published on Web 07/07/2009

If this were true, then there would be a discontinuous change in conductivity of $(1/3)\phi_C\sigma_C$ at the LAM-to-DIS transition. (2) If we imagine the large-amplitude fluctuations to have a locally anisotropic "pancake" shape, then, on average, one-third of the pancakes will be oriented orthogonal to the desired direction of transport, and one recovers $f = 2/3$. If this were true, then there would be no discontinuity in conductivity at the ODT of a LAM phase. (3) If there is extensive mixing of the conducting and nonconducting phases, i.e., the magnitude of the disordered concentration fluctuations is small, then clearly eq 1 is not valid because the presence of the nonconducting component in the conducting phase will affect the intrinsic conductivity of the conducting phase. It is important to note that the magnitude of the concentration fluctuations in the vicinity of the ODT is a strong function of molecular weight[25] and thus one does not expect a universal dependence of conductivity across the ODT in block copolymer/salt mixtures.

One of the problems with determining the presence or absence of a discontinuity in the conductivity of block copolymer electrolytes is the fact that the conductivity of hompolymers (σ_C) is a sensitive function of temperature due to the coupling between segmental motion of the polymer chains and ion transport.[38,39] The Vogel−Tamman−Fulcher (VTF) equation, which is typically used to describe the steep dependence of viscosity on temperature in the vicinity of the glass transition, is often used to describe the temperature-dependent conductivity data from homopolymer samples:[40]

$$\sigma(T) = A \exp\left\{\frac{-B}{R(T-T_0)}\right\} \quad (2)$$

In this expression, σ is the ionic conductivity, A is a constant proportional to the number of charge carriers, B is equivalent to the activation energy for ion motion, R is the gas constant, T is the temperature, and T_0 is a reference temperature which is typically 50 °C above the glass transition temperature of the polymer. Sometimes, a factor of $T^{1/2}$ is added to the preexponential term in order to obtain better fits to the data. The complex nature of the coupling between polymer segments and salt ions makes it impossible to predict the dependence of the VTF parameters on polymer molecular weight, composition, and salt concentration. Thus, σ is a sensitive function of temperature, and deciphering effects due to the temperature dependence of segmental motion and that of morphology may be nontrivial. We circumvent this problem by examining the normalized conductivity, σ_N, defined as

$$\sigma_N = \sigma/(\phi_c\sigma_c) \quad (3)$$

wherein the dependence of conductivity on polymer segmental motion is factored out assuming there is no difference in the temperature dependence of segmental motion in homopolymers and block copolymers. To the extent possible, we will attempt to prove that this assumption is valid for the systems of interest here. If the present framework were valid, then $\sigma_N \equiv f$.

Prior studies indicate that the addition of salts into block copolymers results in a large increase in the ODT temperature. This appears to be a universal result that is valid for copolymers with a wide variety of salt-compatible blocks such as PEO (and PEO derivatives),[3−6] poly(methyl methacrylate),[4,41,42] and poly (vinylpyridine).[43] These studies also show that the size of the microphases and order−order transitions in block copolymers are affected by the presence of salt.

To our knowledge, there are only two previous studies of the effect of ODTs and order−order transitions (OOTs) in amorphous salt/block copolymer mixtures on conductivity. Ruzette et al.[4] found no discontinuity in conductivity at the ODTs in mixtures of poly(methyl methacrylate)-*block*-poly(oligo oxyethylene methacrylate) and lithium trifluoromethanesulfonate ($LiCF_3SO_3$). They, however, reported departures from the VTF expression at the ODT. Cho et al.[3] studied mixtures of a dendrimer−linear chain diblock copolymer and $LiCF_3SO_3$. The copolymer consisted of a PEO linear chain bound to a PEO dendritic core capped with docosyl peripheries. They observed a large discontinuous increase in conductivity when their structures undergo an OOT from hexagonally packed cylinders (the cylinder core was comprised of PEO) to GYR.

The objective of this paper is to report the effect of ODTs and OOTs on the conductivity of mixtures of polystyrene-*block*-poly (ethylene oxide) (SEO) copolymers and lithium bis(trifluoromethylsulfonimide) (LiTFSI). Since the ionic conductivities of crystalline and amorphous PEO phases are dramatically different,[3,38−40,44−46] all reports of structure and conductivity in this paper are restricted to temperatures and salt concentrations where the samples are amorphous.

Table 1. Copolymers Used in This Study

polymer	$M_{n,PS}$ (g/mol)	$M_{n,PEO}$ (g/mol)	φ(PEO block)	PDI
SEO(1.4−2.5)	1400	2500	0.62	1.02
SEO(2.3−4.6)	2300	4600	0.65	1.02
SEO(3.1−5.1)	3100	5100	0.60	1.02
SEO(6.4−7.2)	6400	7200	0.52	1.02

Experimental Section

Materials. The polystyrene-*block*-poly(ethylene oxide) copolymers used in this study were synthesized by sequential living polymerization using the methods described in refs 47, 48, and 49. The polystyrene block was synthesized first using *sec*-butyllithium as the initiator. This was followed by the polymerization of the ethylene oxide with P4 *tert*-butylphosphazene base as a catalyst and then terminated with isopropanol. The copolymers were purified by three filtration and precipitation steps. The molecular weight of the polystyrene block and the polydispersity indices (PDI) of the polystyrene block and overall polymer were obtained by size exclusion chromatography using a Waters 717 plus autosampler and Waters 486 tunable absorbance detector and Wyatt Tech DAWN EOS light-scattering detector calibrated with polystyrene standards. ^{1}H NMR spectroscopy was used to determine the volume fraction of each block. The polymers used in this study, which we call SEO(xx−yy), where xx and yy are the molecular weights of the PS and PEO blocks in kg/mol, respectively, are listed in Table 1. A poly(ethylene oxide) (PEO) homopolymer with a molecular weight of 20 kg/mol (Sigma Aldrich) was used to obtain the intrinsic conductivity of PEO microphases (σ_c).

The procedure for preparing the polymer electrolytes is described in ref 10. We add a predetermined amount of LiTFSI to the copolymers. The salt concentration in our copolymers is quantified by the molar ratio of lithium ions to ethylene oxide moieties, r, which ranges from 0.01 to 0.10.

Morphology Characterization. The structure of the polymer electrolyte was determined by both small-angle X-ray scattering (SAXS) and optical birefringence measurements. Samples for both experiments were prepared by pressing the polymer into sample holders with a 1 mm thick spacer and annealing at 90 °C in a glovebox for 3−5 days. SAXS samples were sealed off in a custom-designed airtight sample holder with Kapton windows while the birefringence samples were sandwiched between two quartz disks and sealed with a silicone-based epoxy. Because of the hygroscopic nature of the salts, glovebox integrity was maintained throughout all stages of experimentation. Measurements were performed at beamline 7.3.3 at the Advanced Light Source (ALS) at Lawrence Berkeley National Laboratories and beamline 15 ID-D at the Advanced Photon Source (APS) at Argonne National Laboratories. Samples were mounted on

a custom-built temperature stage and annealed at each temperature for 20 min before taking measurements. Longer annealing times were not practical due to limited access to the instrumentation. A silver behenate sample was used as a standard, and data were reduced using the Nika program for Igor Pro available from Jan Ilavsky at the APS. The azimuthally averaged scattering intensity, I, is reported as a function of the scattering vector q ($q = 4\pi \sin(\theta/2)/\lambda$, where θ is the scattering angle and λ is the wavelength of the incident beam). At the end of SAXS experiments, Karl Fischer titrations were run on all the samples dissolved in benzene to ensure the samples were dry. The weight fraction of water was less than 0.0015 in all of the samples and, in most cases, comparable to the water content of the benzene used (ca. 5.4 ppm).

Birefringence measurements were performed using the setup described in ref 50 with a plane-polarized beam with wavelength 633 nm as the source. The samples undergo two heating and cooling cycles with temperature steps of ~10 °C. For the heating runs, the sample is annealed at desired temperatures for at least 20 min whereas samples are held at temperatures for 45 min during cooling runs. The intensity of the beam after it passed through the sample and the two crossed polarizers normalized by the incident intensity, I/I_0, was recorded with a photodiode as a function of time and temperature. Karl Fischer titrations were not performed on the birefringence samples due to the difficulty in disassembling the sample holders.

Differential scanning calorimetry (DSC) experiments were conducted on a Thermal Advantage 2920 instrument. SEO/LiTFSI samples were sealed in a Thermal Advantage aluminum hermetic pan in the glovebox. DSC scans were run at 5 °C/min in the range of −30 to 110 °C and cycled (heating and cooling) three times.

Conductivity Measurements. The copolymer/salt mixture was hand-pressed into a pellet and placed at the center of a Garolite spacer with 125 μm thickness and a central hole 3.88 mm in diameter inside a sealed Teflon bag inside the glovebox. A bubble-free disk ca. 150 μm thick was obtained in a heated hand press (110 °C) after about 30 min. The sample was placed between two mirror-polished stainless steel electrodes which were held together by acetal/poly(ether ether ketone) (PEEK) screws and heated to 120 °C in a heated press in the glovebox to ensure good contact between the electrodes and the electrolyte. After determining the final sample thickness using calipers, the electrode−sample assembly without the screws was then placed in a home-built thermostated conductivity cell connected to a Solartron 1260 frequency response analyzer (FRA) with a Solartron 1296 dielectric interface. The complex impedance (Z' and Z'' are the real and imaginary components of the impedance) of the samples were measured using the FRA at 10 °C intervals during heating and cooling scans between 60 and 120 °C. An alternating current (ac) signal ranging from 5 to 100 mV in the frequency range (ω) of 10 Hz−1 MHz was applied to generate the appropriate frequency response. The plateau value in the Bode plot of modulus of the complex impedance, $|Z' + iZ''|$ vs ω, was taken as the sample resistance. This value was nearly identical to the semicircle touchdown on Nyquist Z'' vs Z' plots.

Results and Discussion

Figure 1 shows the SAXS profiles at 69 ± 3 °C for SEO(2.3−4.6) at salt concentrations of $r = 0$, 0.02, 0.05, 0.085, and 0.10. The featureless scattering profile of the pure SEO(2.3−4.6) copolymer ($r = 0$) indicates that the sample is disordered (DIS). A well-defined but broad primary peak at $q^* = 0.57$ nm^{-1} emerges when r is increased to 0.02, indicating the presence of periodic but disordered concentration fluctuations. Increasing r to 0.05 results in a sharpening of the primary peak [full width at half-maximum (fwhm) changes from 0.16 to 0.02 nm^{-1} when r is changed from 0.02 to 0.05], indicating a disorder-to-order transition (DOT) induced by the increase in salt concentration. The higher order peaks at $\sqrt{4}q^*$ and $\sqrt{7}q^*$ at $r = 0.05$ are consistent with the formation of a HEX phase. As more salt is added to the system ($r = 0.085$ and 0.10), the $\sqrt{3}q^*$ peak becomes more prominent, indicating better ordering with increased salt concentration. The volume fraction of the PEO block in the copolymer is 0.65. The addition of salts will undoubtedly change the volume fraction of the polymer (we assume the salt resides solely in the PEO phase). Because of interactions between the salt and the polymer (e.g., coordination between Li^+ and EO moieties), we do not expect the mixing to be ideal. Using ref 51, the relationship between the specific volume of PEO/LiTFSI phase per 1 g PEO as a function salt concentration was developed (ν (cm^3/g) = 0.911 + 3.048*r at 80 °C). These changes in the PEO density, and taking the density of PS as 0.965 g/cm^3, were used to calculate the volume fraction of the PEO phase upon salt addition. Table 2 lists the estimated volume fractions of the PEO-rich microphases for the polymers in this study at selected salt concentrations. For SEO

Table 2. Volume Fractions of Conducting Microphases and Monomer Volumes of SEO/LiTFSI Mixtures Examined in This Study

sample	r	φ_{EO}	volume PEO phase (cm^3/g PEO)
SEO(1.4−2.5)	0.05	0.65	1.06
SEO(2.3−4.6)	0.02	0.66	0.97
	0.05	0.68	1.06
	0.085	0.70	1.17
	0.1	0.71	1.22
SEO(3.1−5.1)	0.03	0.62	1.00
	0.05	0.64	1.06
SEO(6.4−7.2)	0.05	0.56	1.06

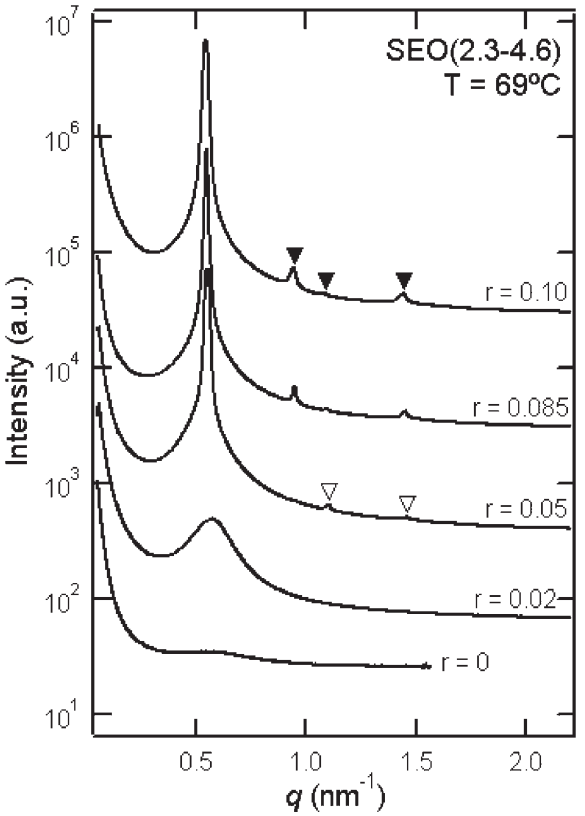

Figure 1. SAXS profiles at 69 ± 3 °C for SEO(2.3−4.6) at $r = 0$, 0.02, 0.05, 0.085, and 0.10. The profiles have been multiplied by 1, 2, 10, 100, and 1000, respectively, to increase the clarity of the plots. Higher order peaks first appear at $r = 0.05$, which are marked with the inverted open triangles at $\sqrt{4}q^*$ and $\sqrt{7}q^*$. Inverted closed triangles mark the higher order peaks at $\sqrt{3}q^*$, $\sqrt{4}q^*$, and $\sqrt{7}q^*$.

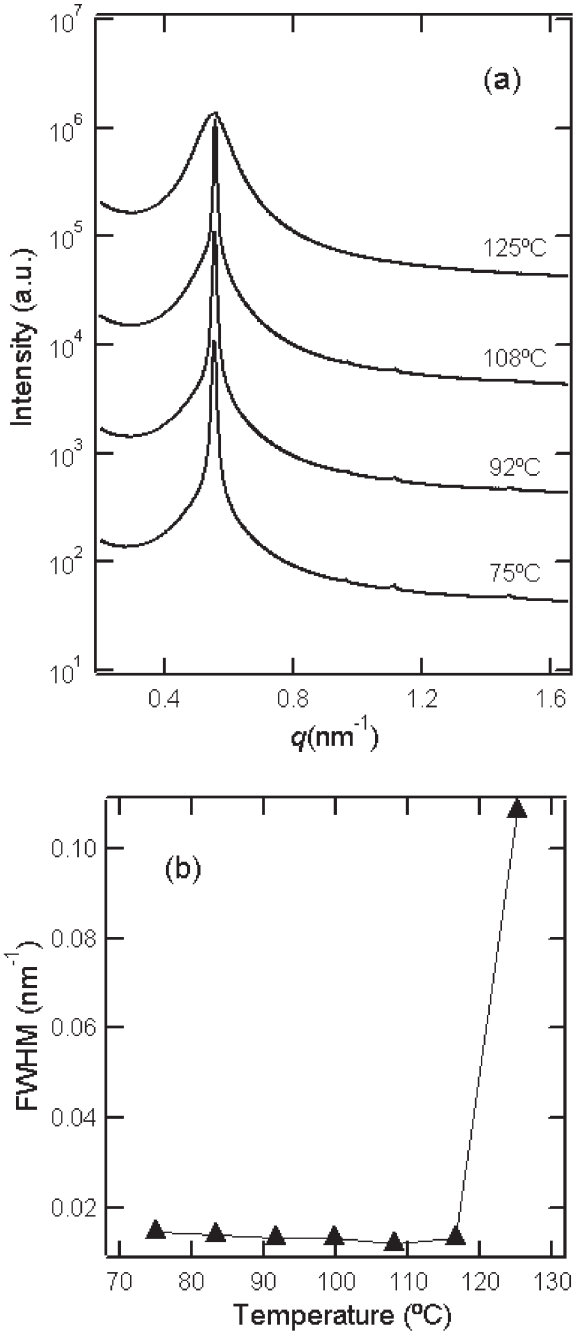

Figure 2. (a) SAXS profiles of SEO(2.3−4.6) at $r = 0.05$ at selected temperatures. The profiles have been multiplied by 1, 10, 100, and 1000, respectively. (b) Plot of the full width half-maximum (fwhm) of the primary peak of the SAXS profiles vs temperature.

(2.3−4.6) at $r = 0.085$ and 0.10, φ_{EO} were estimated to be 0.70 and 0.71, respectively. At these volume fractions, neat block copolymers exhibit hexagonally packed cylinders (HEX) at equilibrium,[2,34] which is consistent with the SAXS data shown in Figure 1. We conclude that SEO(2.3−4.6) exhibits a DIS-to-HEX transition at $r = 0.035 \pm 0.015$ and $T = 69 \pm 3$ °C.

In a similar manner, at $T = 75 \pm 5$ °C we obtain a disordered phase in SEO(3.1−5.1) at $r = 0.02$ and a lamellar phase (LAM) at $r = 0.03$. We conclude that SEO(3.1−5.1) exhibits a DIS-to-LAM transition at $r = 0.025 \pm 0.005$ and $T = 75 \pm 5$ °C. In contrast, the smallest molecular weight polymer, SEO(1.4−2.5), remains disordered up to a salt loading of $r = 0.10$ at all temperatures. Pure SEO(6.4−7.2) has a LAM morphology and exhibits a classic

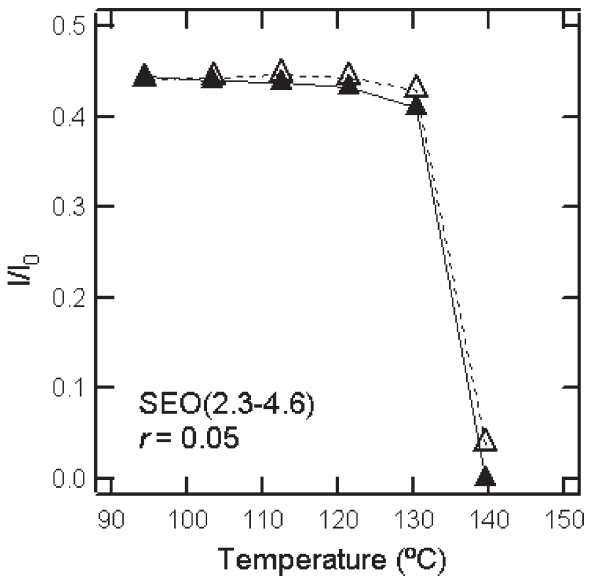

Figure 3. Birefringence signal, I/I_0, vs temperature of SEO(2.3−4.6) at $r = 0.05$. The closed triangles (▲) are data from a heating run, and the open triangles (Δ) are data from a cooling run. The discontinuity between 130 and 140 °C is indicative of an ODT.

LAM-to-DIS transition at 103 ± 5 °C. The data from these samples are not shown explicitly for brevity.

The temperature dependence of SAXS profiles for SEO (2.3−4.6) at $r = 0.05$ is shown in Figure 2. The sample was studied as a function of increasing temperature with 20 min annealing time for equilibration at each temperature. The sample exhibits a HEX phase up to 117 °C. The increase of the fwhm from 0.013 to 0.11 nm^{-1} (Figure 2b) between 117 and 125 °C is indicative of a thermotropic ODT at 121 ± 4 °C. Birefringence experiments were also performed to confirm the presence of an ODT.[52,53] Figure 3 is a plot of the birefringence signal vs temperature from a heating (closed triangles with solid line) and a cooling run (open circles with dashed line). The two runs are in good agreement with each other, indicating reversibility of the ODT in this low molecular weight sample. A discontinuous decrease in the sample birefringence between 130 and 140 °C indicates an ODT at 135 ± 5 °C. The upper limit for the ODT obtained by SAXS is 5 °C lower than the lower limit of the ODT obtained by birefringence. We offer no explanation for this difference. We repeated the birefringence measurements on an independent sample and got the same ODT given above. SAXS experiments were not repeated due to limited equipment access.

Figure 4 shows the temperature dependence of the SAXS profiles for SEO(3.1−5.1) at $r = 0.03$. A narrow primary peak at $q^* = 0.49$ nm^{-1} and a higher order peak at $2q^*$, characteristic of a LAM phase, are obtained at 66 °C. Although the $2q^*$ peak is no longer visible at 83 °C, the primary peak remains nearly as narrow as that at 66 °C. Increasing the sample temperature from 83 to 92 °C results in a discontinuous increase of the fwhm of the primary peak from 0.017 to 0.072 nm^{-1} (see Figure 4b), signifying an ODT at 87.5 ± 5 °C. Figure 5 is a plot of the birefringence measurement from a cooling run on SEO(3.1−5.1) at $r = 0.03$. The discontinuous decrease in intensity between 87 and 97 °C indicates an ODT at 92 ± 5 °C. The ODT temperatures measured by SAXS and birefringence for this sample are in good agreement with each other.

Using the three different SEO polymers with accessible ODTs, SEO(6.4−7.2) at $r = 0$, SEO(3.1−5.1) at $r = 0.03$, and SEO(2.3−4.6) at $r = 0.05$, we can develop a relationship to estimate the

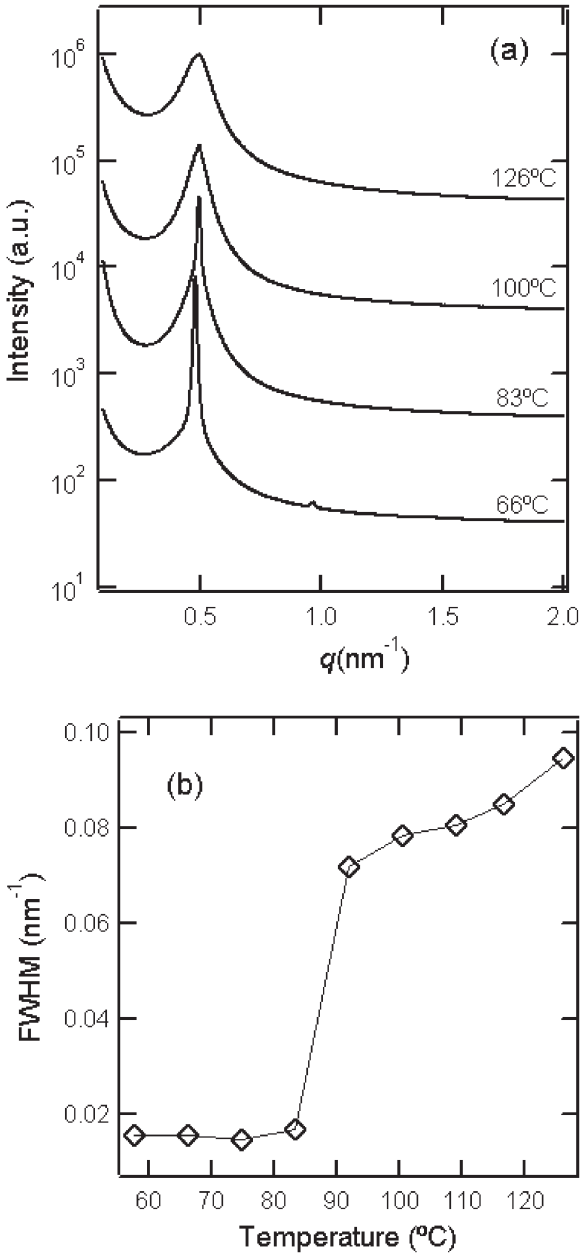

Figure 4. (a) SAXS profiles of SEO(3.1−5.1) at $r = 0.03$ at selected temperatures. The profiles have been multiplied by 1, 10, 100, and 1000, respectively. (b) Plot of the full width half-maximum (fwhm) of the primary peak from the SAXS profiles vs temperature.

change in the effective Flory−Huggins chi parameter, χ_{eff}, with salt concentration. Leibler's theory[24] can be used to predict the χ at the ODT:

$$(\chi_{eff}N)_{ODT} = S \quad (4)$$

where $N = (v_{PS}/v_0)N_{PS} + (v_{PEO}/v_0)N_{PEO}$, using $v_0 = 0.1$ nm^3, v_{PEO} is the volume of the PEO/LiTFSI microphase per PEO monomer, calculated on the basis of the data tabulated in Table 2, and S is a constant that depends on ϕ_{EO} (e.g., $S = 10.5$ for $\phi_{EO} = 0.5$). Ignoring the temperature dependence of χ, eq 4 is applied to the ODT data of the three block copolymers listed above and plotted in Figure 6. The estimated value of χ_{eff} for the neat SEO is in good agreement with literature for $T = 95$ °C.[54] It is clear that even the addition of a small amount of salt ($r = 0-0.05$, which corresponds to 1 Li^+ per 20 EO moieties) significantly increases χ_{eff}.

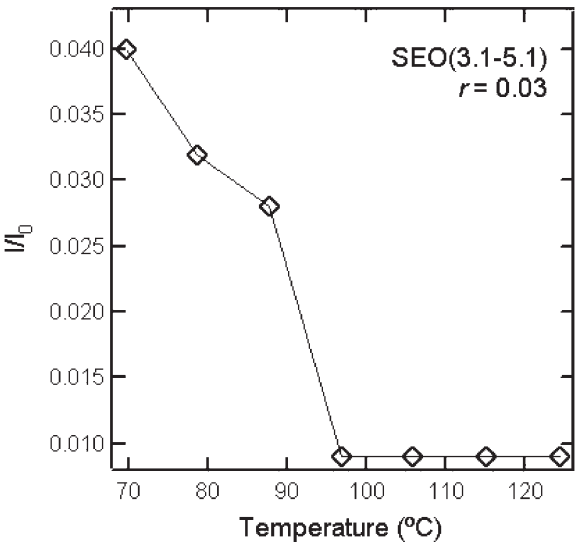

Figure 5. Birefringence signal, I/I_0, vs temperature of SEO(3.1−5.1) at $r = 0.03$ during a cooling run.

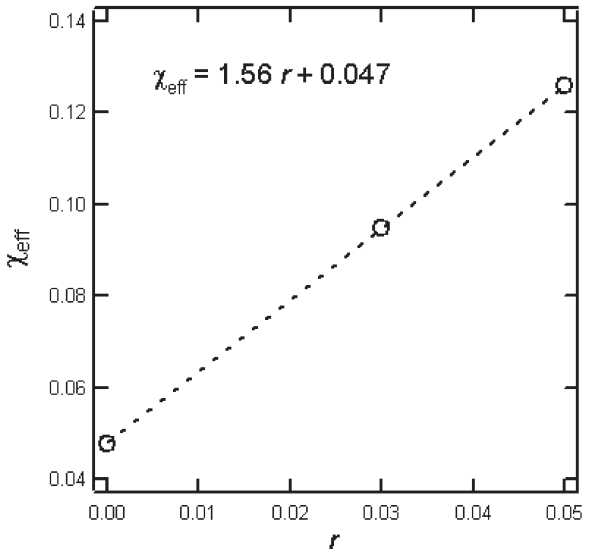

Figure 6. Plot of χ_{eff} vs salt concentration. The values of χ_{eff} were determined using Leibler's theory at the order−disorder transition for SEO(6.4−7.2) at $r = 0$, SEO(3.1−5.1) at $r = 0.03$, and SEO(2.3−4.6) at $r = 0.05$.

The temperature dependence of SAXS profiles for SEO(3.1−5.1) with $r = 0.05$ is shown in Figure 7. The higher order peaks at $2q^*$ and $3q^*$ seen at 59 °C (marked by arrows) indicate the presence of a LAM morphology. When the sample temperature is increased to 77 °C, the primary peak shifts from 0.456 to 0.475 nm^{-1}. Further increase in sample temperature to 94 °C results in the appearance of a new higher order peak at $q = 0.548$ nm^{-1}. In addition, the higher order peak at $2q^*$ persists (see inset of Figure 7). Further increase in sample temperature leads to an increase in the intensity of the higher order peak at $q = 0.548$ nm^{-1} and a reduction in the intensity of the peak at $2q^*$. The peaks at 137 °C are readily indexed as q^*, $(4/3)^{1/2}q^*$, and $(7/3)^{1/2}q^*$, characteristic of scattering from a gyroid (GYR) phase. The SAXS data at temperatures between 77 and 137 °C show coexisting LAM and GYR phases. DSC data reveal that SEO(3.1−5.1) at $r = 0.05$ has a melting temperature of 42 °C and a crystallization temperature of 6 °C, well below the temperature range of the SAXS experiments. We thus do not believe that the LAM phase in our system is induced by

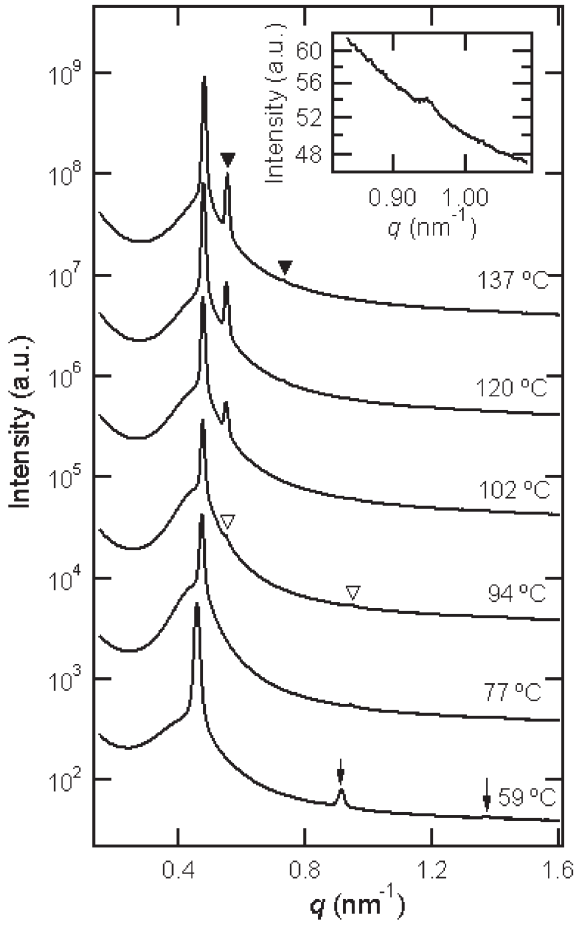

Figure 7. SAXS profiles of SEO(3.1−5.1) at $r = 0.05$ at selected temperatures. The profiles have been multiplied by 1, 10, 100, 1000, and 10000. The arrows mark higher order peaks at $2q^*$ and $3q^*$, indicating a lamellar structure at 59 °C. The closed inverted triangles mark higher order peaks at $(4/3)^{1/2}q^*$ and $(7/3)^{1/2}q^*$, indicating a gyroid structure at 137 °C. The open inverted triangles mark where the $(4/3)^{1/2}q^*$ peak for a gyroid structure first appears and the persisting $2q^*$ peak for a lamellar structure. The inset is an enlargement of the 94 °C profile to increase the clarity of the observed $2q^*$ peak.

crystallization as has been reported for different SEO copolymers in refs 54 and 55.

Birefringence can be used to study the LAM−GYR OOT because the LAM phase is birefringent while the GYR phase is not.[55−57] Equilibrated birefringence data obtained from SEO (3.1−5.1) with $r = 0.05$ after step increases in sample temperature are shown in Figure 8. The birefringence signal decreases continuously over a temperature range from 52 to 106 °C and is independent of temperature at temperatures above 106 °C. This is in contrast to previous birefringence studies of gyroid phases in diblock copolymer solutions where discontinuous changes in the signal were seen at the OOT.[55−57] The time dependence of the birefringence signal obtained after step decreases in temperature is shown in Figure 9. Above 106 °C the birefringence signal is low and insensitive to changes in temperature, except for a small overshoot at the beginning of temperature jumps. At temperatures below 106 °C, the birefringence increases after the temperature is lowered in the first 10 min or so after the quench and then reaches a time-independent plateau. We interpret the increase in signal to reflect conversion of some of the GYR grains into LAM. The coexistence of LAM and GYR at the phase boundary between the LAM and GYR phases is required by the Gibbs phase rule for binary mixtures. This coexistence may reflect the preferential partitioning of salt ions in either LAM or GYR phases. On the

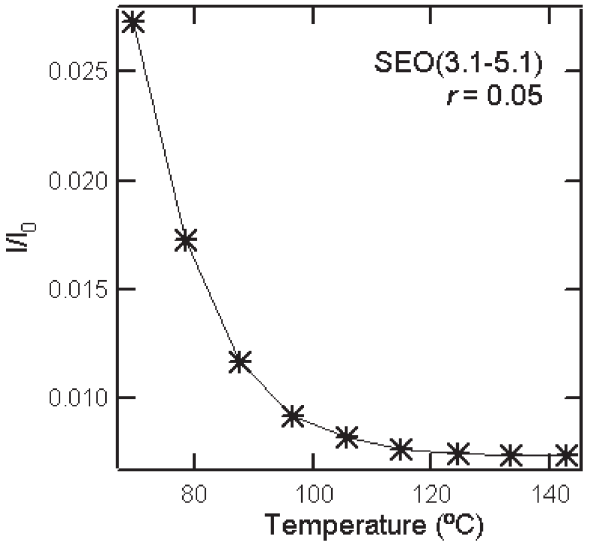

Figure 8. Birefringence signal, I/I_0, vs temperature of SEO(3.1−5.1) at $r = 0.05$ during a cooling run.

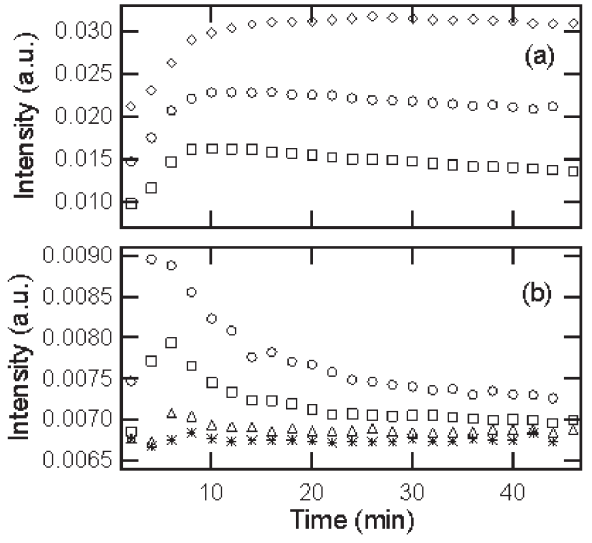

Figure 9. Birefringence signal, I/I_0, vs time for SEO(3.1−5.1) at $r = 0.05$ for a cooling run at low temperatures (a), where squares (□) are data for temperature changes of 88 °C → 78 °C, circles (○) are 78 °C → 70 °C, and diamonds (◇) are 70 °C → 60 °C, and high temperatures (b) where asterisks (∗) are 142 °C → 133 °C, triangles (Δ) are 133 °C → 124 °C, squares (□) are 124 °C → 114 °C, and circles (○) are 114 °C → 106 °C.

other hand, the coexistence of LAM and GYR may reflect the slow kinetics of OOTs involving the GYR phase, as has been noted in previous studies on pure diblock copolymers.[32,33]

The magnitude of the birefringence signal, I/I_0, of SEO(3.1−5.1) at $r = 0.03$ (Figure 3) with a cylindrical ordered morphology is about an order of magnitude larger than that of the lamellar samples [SEO(3.1−5.1) with $r = 0.03$ and $r = 0.05$; Figures 5 and 8]. The birefringence signals depend on the geometry of the microphase, the optical contrast between the microphases, and the grain structure.[58,59] Determining these factors is outside the scope of this paper.

In some cases, it appears as if the primary peak in the SAXS profiles is a summation of a broad peak and a narrow peak. An example of this is shown in Figure 10a where we show data obtained from SEO(2.3−4.6) at $r = 0.05$ at 117 °C. There are at least two possible explanations for this observation.

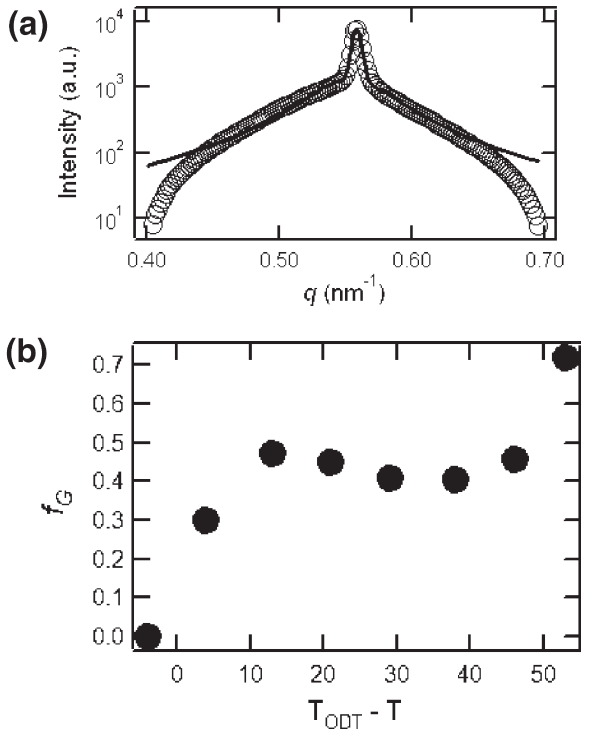

Figure 10. (a) Background-subtracted SAXS intensity $I - I_b$ vs scattering vector q of SEO(2.3−4.6) at $r = 0.05$ at $T = 117$ °C. The symbols represent the data and the curve is a least-squares fit to eq 5. (b) Fraction of the scattering invariant attributed to the sharp Gaussian peak, f_G, of SEO(2.3−4.6) at $r = 0.05$, plotted against $T_{ODT} - T$.

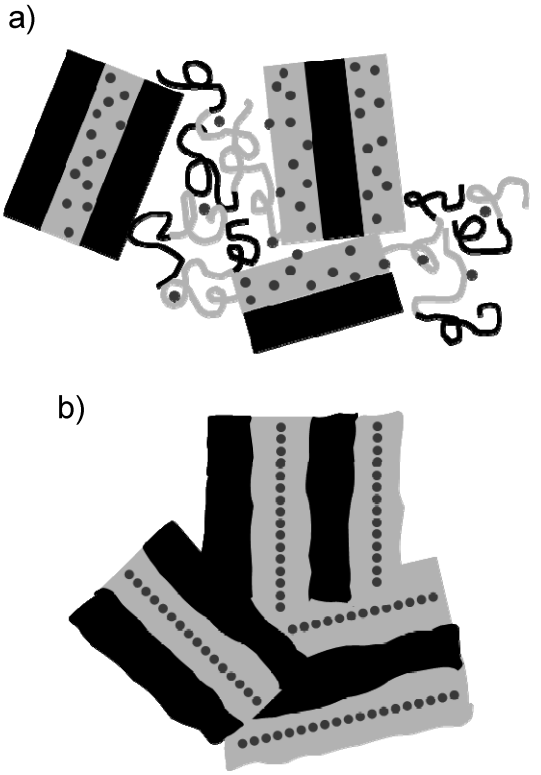

Figure 11. Schematic representations of two possible scenarios for the structure of weakly ordered SEO/LiTFSI mixtures. Light gray corresponds to the PEO phase, black corresponds to the PS phase, and medium gray circles represent LiTFSI. (a) Coexistence of an ordered and disordered phase. (b) Thin well-ordered lithium channels within poorly ordered PEO domains.

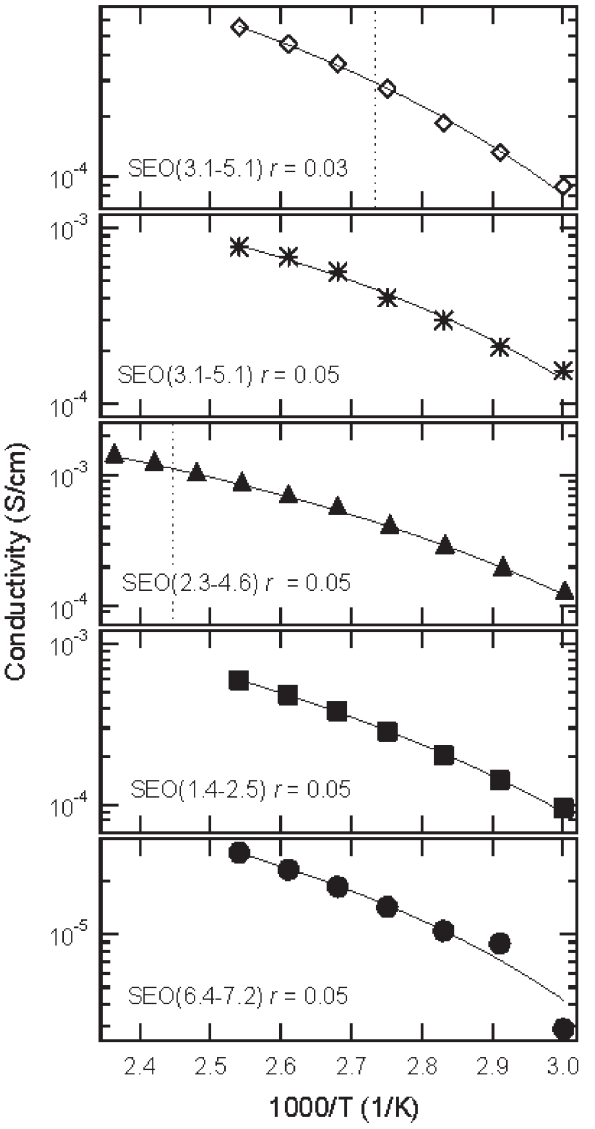

Figure 12. Plot of conductivity vs $1000/T$ for SEO(6.4−7.2), SEO(1.4−2.5), SEO(2.3−4.6), and SEO(3.1−5.1) all at $r = 0.05$ and SEO(3.1−5.1) at $r = 0.03$. The lines through the data points are VTF fits. Dashed vertical lines mark locations of the ODT's.

(1) A coexistence of a disordered phase and an ordered phase, accompanied by a partitioning of the salt in the ordered domains as depicted in Figure 11a. In this case, the disordered phase would contribute to the broad peak while the ordered phase would contribute to the narrow peak. Since the volume fraction of the ordered phase is expected to increase with quench depth below the ODT, we would expect the contribution due to the narrow peak to increase rapidly as $T_{ODT} - T$ increases. (2) All of the sample is ordered, but the lithium is not uniformly distributed in the PEO microphase as depicted in Figure 11b. If the lithium-rich domains were more ordered than the PEO domains as shown schematically in Figure 11b, then they would contribute to the sharp peak while the block copolymer microphases would contribute to the broad peak. Evidence for the nonuniform distribution of lithium in PEO microphases of SEO/LiTFSI mixtures has been optimized by energy-filtered transmission electron microscopy images.[60] For this scenario, the fraction of the SAXS signal attributable to the narrow peak would be independent of quench depth.

In an attempt to resolve which explanation is correct, a summation of a sharp Gaussian peak and a broad Lorentzian

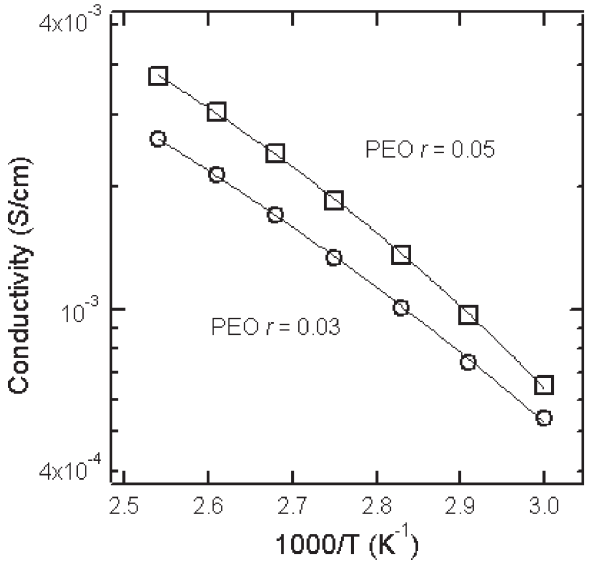

Figure 13. Plot of conductivity vs 1000/T for a 20 kg/mol PEO homopolymer at $r = 0.03$ (○) and $r = 0.05$ (□). Solid lines through the data points are VTF fits.

peak is fit to the primary peak after subtracting a decaying background.

$$I(q) - I_b = A_1 \exp\left(\frac{-(x_1 - q)^2}{{c_1}^2}\right) + \left(\frac{A_2}{1 + \left(\frac{x_2 - q}{c_2}\right)^2}\right) \qquad (5)$$

The first expression on the right-hand side is the Gaussian, $G(q)$, contribution while the second term is the Lorentzian, $L(q)$, contribution. The background term was determined by fitting the equation $I_b = I_0 + A_0 \exp(-q/c_0)$ to the data with the peak masked, using I_0, A_0, and c_0 as the fitting parameters. The resulting $I(q) - I_b$ data were fit to eq 5 with A_1, A_2, x_1, x_2, c_1, and c_2 as fitting parameters. The relative contributions from the Gaussian and Lorentzian peaks were determined by numerically evaluating the invariant $\int G(q)q^2\,dq$ and $\int L(q)q^2\,dq$. For SEO (2.3−4.6) at $r = 0.05$, the limits of the integration were from 0.40 to 0.70 nm^{-1}. The fraction of the invariant under the Gaussian peak, f_G, for this sample is plotted versus $T_{ODT} - T$ in Figure 10b. It is clear that $f_G = 0.45 \pm 0.05$ at temperatures 10−50 °C below T_{ODT}, and it rapidly approaches 0 when the temperature is within 10 °C of T_{ODT}. The data in Figure 10b thus lend support to scenario (2) depicted in Figure 11b. The birefringence data in Figure 3 also lend support to this conclusion. We hope to further clarify the nature of the salt-induced ODTs and OOTs in block copolymers in future experiments, especially for complex cases like SEO(3.1−5.1) at $r = 0.05$ where two sharp peaks are superposed on a broader peak (Figure 7).

Plots of the temperature dependence on σ for selected SEO/salt mixtures are shown in Figure 12. We have included data from SEO(6.4−7.2) at $r = 0.05$ which is LAM at all temperatures, SEO (1.4−2.5) at $r = 0.05$ which is DIS at all temperatures, SEO(2.3−4.6) at $r = 0.05$ which exhibited a HEX-to-DIS transition at 135 °C, SEO(3.1−5.1) at $r = 0.03$ which exhibited a LAM-to-DIS transition at 92 °C, and SEO (3.1−5.1) at $r = 0.05$ which exhibited a gradual LAM-to-GYR transition between 52 and 106 °C. The solid lines through the data are VTF fits (eq 2) with A, B, and T_0 as fitting parameters. We leave T_0 floating since the T_g of the polymer is a function of the salt concentration and molecular weight. It is of interest to note that the VTF equation fits the full data set showing no deviations at phase transitions.

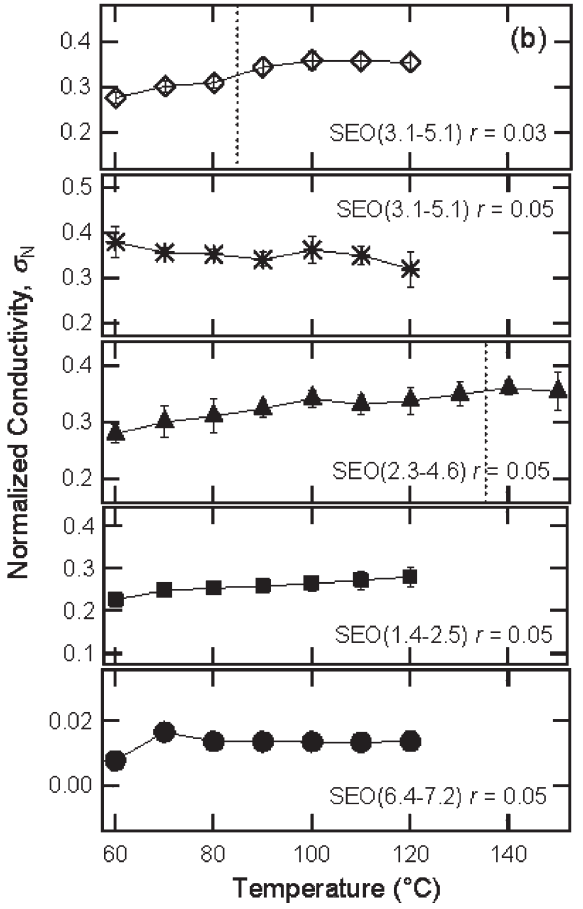

Figure 14. Plot of normalized conductivity (as calculated from eq 3) vs temperature for SEO(6.4−7.2), SEO(1.4−2.5), SEO(2.3−4.6), and SEO (3.1−5.1) all at $r = 0.05$ and SEO(3.1−5.1) at $r = 0.03$. The dashed vertical lines mark the ODT.

In order to focus on the effect of the morphological phase transitions on conductivity, we calculated σ_N using the conductivity data in Figure 12 and eq 3. The measured conductivity of PEO homopolymer as a function of r and T is shown in Figure 13. These measurements were made up to 120 °C, and extrapolations based on VTF fits through the data were used to estimate σ_c at higher temperatures. Lascaud et al.[61] measured the conductivity of mixtures of a 4 kg/mol PEO and LiTFSI as a function of salt concentrations and temperatures. The conductivity of this sample was somewhat higher than that of our 20 kg/mol PEO conductivity data due to well-established effects arising from differences in molecular weight, but the temperature dependence of the conductivities of the two sets of samples were similar. For consistency, we have used our measurements to compute σ_N.

The values of σ_N of SEO(1.4−2.5), $r = 0.05$, which is disordered in the temperature range of interest, and SEO(6.4−7.2), $r = 0.05$, which has a LAM morphology in the temperature range of interest, are 0.259 ± 0.017 and 0.013 ± 0.002, respectively, and have negligible dependence on temperature. The lack of dependence of σ_N on temperature for these widely different samples indicates that our normalization scheme accounts for the temperature dependence of ion transport due to the temperature dependence of segmental motion in SEO copolymers in the absence of phase transitions. The fact that the presence of polystyrene segments does not affect σ_N of SEO(1.4−2.5) with $r = 0.05$ indicates that the conducting pathways in the DIS phase are primarily PEO-rich domains that are qualitatively similar to those obtained in the ordered state. It is, perhaps, surprising that

the dependence of σ_N on temperature is also weak for the three samples that exhibited phase transitions in the accessible temperature window (Figure 13). There seems to be a subtle increase in σ_N of SEO(3.1−5.1) at $r = 0.03$ between 60 and 90 °C, before leveling off at about 0.35 at temperatures above 100 °C. The SEO (3.1−5.1), $r = 0.03$, sample exhibits an ODT at 92 °C (denoted by dashed line in Figure 14) which makes it tempting to conclude that the slight changes in the temperature dependence of σ_N seen in the vicinity of the ODT is due to this. However, SEO(2.3−4.6), $r = 0.05$, with an ODT at about 135 °C also exhibits similar behavior in the vicinity of 100 °C. The subtle changes seen in the temperature dependencies of σ_N in samples with accessible ODTs thus cannot be attributed to morphological transitions. In the ordered state, the polymer chains are part of a quasi-static solid morphology, while in the disordered state, the polymer chains diffuse freely with relatively few thermodynamic barriers.[62] The lack of sensitivity of σ_N on the location of the ODT indicates that ion transport is only affected by segmental motion, not chain motion in copolymers with molecular weights as low as 7 kg/mol.

The σ_N values of SEO(3.1−5.1), $r = 0.05$, the samples that exhibits a LAM-to-GYR transition at temperatures between 52 and 106 °C, are scattered between 0.32 and 0.38. It is evident that this OOT also has no effect on ionic conductivity.

We note in passing that the estimated glass transition temperatures of the polystyrene homopolymers with molecular weights equal to those of the polystyrene blocks in our SEO copolymers with accessible phase transitions range from 45 to 52 °C.[63] All of our measurements were conducted at temperatures above 52 °C. We were unable to detect the glass transition in DSC scans of our SEO samples.

It is clear that our data do not support the arguments presented in the Introduction where we defined the morphology factor, f. For example, if our arguments were correct, then σ_N would increase by 50%, from 0.67 to 1.0, at the LAM-to-GYR transition (Figure 14). Instead, we observe that σ_N is unaffected by this transition and is scattered around an average value of 0.35. Our experiments indicate that the there is no difference in the morphology factors of LAM and GYR phases. In the only related study that we are aware of, Cho et al. report a jump in ionic conductivity from 1.8×10^{-5} to 1.5×10^{-4} S/cm at the HEX-to-GYR transition in their copolymer.[3] Since Cho et al. did not measure σ_C, it is not possible to estimate σ_N for their sample. However, on the basis of morphology factors defined in the Introduction, one expects a 3-fold increase in conductivity at the HEX-to-GYR transition (σ_N increasing from 0.33 to 1.00), which is inconsistent with the observation of Cho et al. There is thus a fundamental discrepancy between the present observation that conductivity is not affected by the LAM-to-GYR transition and the conclusion of Cho et al. that conductivity is affected by the HEX-to-GYR transition. At this point it is unclear whether this difference arises from different polymer systems, salts, grain sizes, or other effects. Further work is needed to resolve the discrepancy between these two studies.

In the Introduction, we described how f (or, equivalently, σ_N) is expected to vary across ODTs. The lack of change in σ_N at both the HEX-to-DIS and LAM-to-DIS transitions indicates that PEO-rich fluctuations provide the primary pathways for ion conduction and that these pathways are similar to those found in the ordered state. Our results differ substantially from those of Ruzette et al.,[4] who found that the conductivity of mixtures of a symmetric poly(methyl methacrylate)-*block*-poly(oligo oxyethylene methacrylate) (PMMA−POEM) and lithium trifluoromethanesulfonate ($LiCF_3SO_3$) was consistent with the VTF expression in the ordered state but not in the disordered state. In contrast, our data are consistent with the VTF equation in both the ordered and disordered states (Figure 12). The molecular weight of the copolymer used by Ruzette et al. (80 kg/mol) is significantly larger than that of the copolymers used in this study (10 kg/mol). The discontinuity of the order parameter at the ODT in symmetric block copolymers decreases with increasing molecular weight.[25] On the basis of this fact, one would expect more pronounced effect of the ODT on conductivity in our SEO copolymers than that in PMMA−POEM. The difference in molecular weight of the samples used in the two studies thus cannot account for the observed differences.

Conclusion

We have created a set of SEO/LiTFSI mixtures with accessible order−disorder and order−order transitions. SEO(2.3−4.6) with $r = 0.05$ exhibited a HEX-to-DIS transition at about 135 °C, while SEO(3.1−5.1) with $r = 0.03$ exhibited a LAM-to-DIS at 92 °C. A gradual LAM-to-GYR transition was observed for SEO(3.1−5.1) with $r = 0.03$ at temperatures between 52 and 106 °C. The temperature dependence of the conductivity of these samples was consistent with the Vogel−Tamman−Fulcher equation, in spite of the presence of the above-mentioned phase transitions. The ionic conductivities of the SEO/LiTFSI samples, normalized by the ionic conductivity of a 20 kg/mol homopolymer PEO sample at the salt concentration and temperature of interest, were independent of temperature. We conclude that order−order and order−disorder transitions have no effect on ionic conductivity in the limited SEO samples that we have examined thus far. In contrast, all previous studies of ionic conductivity in block copolymer/salt mixtures have concluded that conductivity is affected by both order−order and order−disorder transitions.

Acknowledgment. This work was conducted within the Batteries for Advanced Transportation Technologies (BATT) Program, supported by the U.S. Department of Energy FreedomCAR and Vehicle Technologies Program. N.S.W. was supported by a National Science Foundation Graduate Research Fellowship. The Advanced Light Source is supported by the Director, Office of Science, Office of Basic Energy Sciences, of the U.S. Department of Energy under Contract DE-AC02-05CH11231. ChemMatCARS Sector 15 is principally supported by the National Science Foundation/Department of Energy under Grant CHE-0535644. Use of the Advanced Photon Source was supported by the U.S. Department of Energy, Office of Science, Office of Basic Energy Sciences, under Contract DE-AC02-06CH11357. We thank Dr. Enrique Gomez for helpful discussions.

References and Notes

(1) Tarascon, J. M.; Armand, M. *Nature (London)* **2001**, *414* (6861), 359–367.
(2) Floudas, G.; Vazaiou, B.; Schipper, F.; Ulrich, R.; Wiesner, U.; Iatrou, H.; Hadjichristidis, N. *Macromolecules* **2001**, *34* (9), 2947–2957.
(3) Cho, B. K.; Jain, A.; Gruner, S. M.; Wiesner, U. *Science* **2004**, *305* (5690), 1598–1601.
(4) Ruzette, A. V. G.; Soo, P. P.; Sadoway, D. R.; Mayes, A. M. *J. Electrochem. Soc.* **2001**, *148* (6), A537–A543.
(5) Epps, T. H.; Bailey, T. S.; Pham, H. D.; Bates, F. S. *Chem. Mater.* **2002**, *14* (4), 1706–1714.
(6) Epps, T. H.; Bailey, T. S.; Waletzko, R.; Bates, F. S. *Macromolecules* **2003**, *36* (8), 2873–2881.
(7) Soo, P. P.; Huang, B. Y.; Jang, Y. I.; Chiang, Y. M.; Sadoway, D. R.; Mayes, A. M. *J. Electrochem. Soc.* **1999**, *146* (1), 32–37.
(8) Trapa, P. E.; Acar, M. H.; Sadoway, D. R.; Mayes, A. M. *J. Electrochem. Soc.* **2005**, *152* (12), A2281–A2284.
(9) Trapa, P. E.; Huang, B. Y.; Won, Y. Y.; Sadoway, D. R.; Mayes, A. M. *Electrochem. Solid State Lett.* **2002**, *5* (5), A85–A88.
(10) Singh, M.; Odusanya, O.; Wilmes, G. M.; Eitouni, H. B.; Gomez, E. D.; Patel, A. J.; Chen, V. L.; Park, M. J.; Fragouli, P.; Iatrou, H.; Hadjichristidis, N.; Cookson, D.; Balsara, N. P. *Macromolecules* **2007**, *40* (13), 4578–4585.

(11) Park, M. J.; Balsara, N. P. *Macromolecules* **2008**, *41* (10), 3678–3687.
(12) Elabd, Y. A.; Napadensky, E.; Walker, C. W.; Winey, K. I. *Macromolecules* **2006**, *39* (1), 399–407.
(13) Elabd, Y. A.; Walker, C. W.; Beyer, F. L. *J. Membr. Sci.* **2004**, *231* (1−2), 181–188.
(14) Niitani, T.; Shimada, M.; Kawamura, K.; Dokko, K.; Rho, Y. H.; Kanamura, K. *Electrochem. Solid State Lett.* **2005**, *8* (8), A385–A388.
(15) Niitani, T.; Shimada, M.; Kawamura, K.; Kanamura, K. *J. Power Sources* **2005**, *146* (1−2), 386–390.
(16) Ioannou, E. F.; Mountrichas, G.; Pispas, S.; Kamitsos, E. I.; Floudas, G. *Macromolecules* **2008**, *41* (16), 6183–6190.
(17) Thurn-Albrecht, T.; DeRouchey, J.; Russell, T. P.; Jaeger, H. M. *Macromolecules* **2000**, *33* (9), 3250–3253.
(18) Thurn-Albrecht, T.; DeRouchey, J.; Russell, T. P.; Kolb, R. *Macromolecules* **2002**, *35* (21), 8106–8110.
(19) Tsori, Y.; Tournilhac, F.; Andelman, D.; Leibler, L. *Phys. Rev. Lett.* **2003**, *90* (14).
(20) Tsori, Y.; Tournilhac, F.; Leibler, L. *Macromolecules* **2003**, *36* (15), 5873–5877.
(21) Xu, T.; Zhu, Y. Q.; Gido, S. P.; Russell, T. P. *Macromolecules* **2004**, *37* (7), 2625–2629.
(22) Xu, T.; Zvelindovsky, A. V.; Sevink, G. J. A.; Gang, O.; Ocko, B.; Zhu, Y. Q.; Gido, S. P.; Russell, T. P. *Macromolecules* **2004**, *37* (18), 6980–6984.
(23) Xu, T.; Zvelindovsky, A. V.; Sevink, G. J. A.; Lyakhova, K. S.; Jinnai, H.; Russell, T. P. *Macromolecules* **2005**, *38* (26), 10788–10798.
(24) Leibler, L. *Macromolecules* **1980**, *13* (6), 1602–1617.
(25) Fredrickson, G. H.; Helfand, E. *J. Chem. Phys.* **1987**, *87* (1), 697–705.
(26) Floudas, G.; Ulrich, R.; Wiesner, U. *J. Chem. Phys.* **1999**, *110* (1), 652–663.
(27) Bates, F. S.; Fredrickson, G. H. *Phys. Today* **1999**, *52* (2), 32–38.
(28) Matsen, M. W.; Bates, F. S. *Macromolecules* **1996**, *29* (4), 1091–1098.
(29) Matsen, M. W.; Bates, F. S. *J. Chem. Phys.* **1997**, *106* (6), 2436–2448.
(30) Matsen, M. W.; Bates, F. S. *J. Polym. Sci., Part B: Polym. Phys.* **1997**, *35* (6), 945–952.
(31) Khanna, V.; Cochran, E. W.; Hexemer, A.; Stein, G. E.; Fredrickson, G. H.; Kramer, E. J.; Li, X.; Wang, J.; Hahn, S. F. *Macromolecules* **2006**, *39* (26), 9346–9356.
(32) Hajduk, D. A.; Takenouchi, H.; Hillmyer, M. A.; Bates, F. S.; Vigild, M. E.; Almdal, K. *Macromolecules* **1997**, *30* (13), 3788–3795.
(33) Hajduk, D. A.; Harper, P. E.; Gruner, S. M.; Honeker, C. C.; Kim, G.; Thomas, E. L.; Fetters, L. J. *Macromolecules* **1994**, *27* (15), 4063–4075.
(34) Khandpur, A. K.; Forster, S.; Bates, F. S.; Hamley, I. W.; Ryan, A. J.; Bras, W.; Almdal, K.; Mortensen, K. *Macromolecules* **1995**, *28* (26), 8796–8806.
(35) Bates, F. S.; Schulz, M. F.; Khandpur, A. K.; Forster, S.; Rosedale, J. H.; Almdal, K.; Mortensen, K. *Faraday Discuss.* **1994**, *98* (98), 7–18.
(36) Lodge, T. P.; Blazey, M. A.; Liu, Z.; Hamley, I. W. *Macromol. Chem. Phys.* **1997**, *198* (4), 983–995.
(37) Sax, J.; Ottino, J. M. *Polym. Eng. Sci.* **1983**, *23* (3), 165–176.
(38) Kakihana, M.; Schantz, S.; Torell, L. M. *J. Chem. Phys.* **1990**, *92* (10), 6271–6277.
(39) Watanabe, M.; Sanui, K.; Ogata, N.; Kobayashi, T.; Ohtaki, Z. *J. Appl. Phys.* **1985**, *57* (1), 123–128.
(40) Gray, F. M. *Polymer Electrolytes*; The Royal Society of Chemistry: Cambridge, 1997; p 175.
(41) Wang, J. Y.; Chen, W.; Roy, C.; Sievert, J. D.; Russell, T. P. *Macromolecules* **2008**, *41* (3), 963–969.
(42) Wang, J. Y.; Chen, W.; Russell, T. P. *Macromolecules* **2008**, *41* (13), 4904–4907.
(43) Lee, D. H.; Kim, H. Y.; Kim, J. K.; Huh, J.; Ryu, D. Y. *Macromolecules* **2006**, *39* (6), 2027–2030.
(44) Volel, M.; Armand, M.; Gorecki, W. *Macromolecules* **2004**, *37* (22), 8373–8380.
(45) Boden, N.; Leng, S. A.; Ward, I. M. *Solid State Ionics* **1991**, *45* (3−4), 261–270.
(46) Croce, F.; Appetecchi, G. B.; Persi, L.; Scrosati, B. *Nature (London)* **1998**, *394* (6692), 456–458.
(47) Hadjichristidis, N.; Iatrou, H.; Pispas, S.; Pitsikalis, M. *J. Polym. Sci., Part A: Polym. Chem.* **2000**, *38* (18), 3211–3234.
(48) Quirk, R. P.; Kim, J.; Kausch, C.; Chun, M. S. *Polym. Int.* **1996**, *39* (1), 3–10.
(49) Esswein, B.; Moller, M. *Angew. Chem., Int. Ed. Engl.* **1996**, *35* (6), 623–625.
(50) Garetz, B. A.; Newstein, M. C.; Dai, H. J.; Jonnalagadda, S. V.; Balsara, N. P. *Macromolecules* **1993**, *26* (12), 3151–3155.
(51) Edman, L.; Doeff, M. M.; Ferry, A.; Kerr, J.; De Jonghe, L. C. *J. Phys. Chem. B* **2000**, *104* (15), 3476–3480.
(52) Balsara, N. P.; Garetz, B. A.; Dai, H. J. *Macromolecules* **1992**, *25* (22), 6072–6074.
(53) Balsara, N. P.; Perahia, D.; Safinya, C. R.; Tirrell, M.; Lodge, T. P. *Macromolecules* **1992**, *25* (15), 3896–3901.
(54) Zhu, L.; Cheng, S. Z. D.; Calhoun, B. H.; Ge, Q.; Quirk, R. P.; Thomas, E. L.; Hsiao, B. S.; Yeh, F.; Lotz, B. *Polymer* **2001**, *42* (13), 5829–5839.
(55) Lodge, T. P.; Hanley, K. J.; Pudil, B.; Alahapperuma, V. *Macromolecules* **2003**, *36* (3), 816–822.
(56) Hanley, K. J.; Lodge, T. P.; Huang, C. I. *Macromolecules* **2000**, *33* (16), 5918–5931.
(57) Lodge, T. P.; Pudil, B.; Hanley, K. J. *Macromolecules* **2002**, *35* (12), 4707–4717.
(58) Kim, W. G.; Chang, M. Y.; Garetz, B. A.; Newstein, M. C.; Balsara, N. P.; Lee, J. H.; Hahn, H.; Patel, S. S. *J. Chem. Phys.* **2001**, *114* (22), 10196–10211.
(59) Newstein, M. C.; Garetz, B. A.; Dai, H. J.; Balsara, N. P. *Macromolecules* **1995**, *28* (13), 4587–4597.
(60) Gomez, E. D.; Panday, A.; Feng, E. H.; Chen, V.; Stone, G. M.; Minor, A. M.; Kisielowski, C.; Downing, K. H.; Borodin, O.; Smith, G. D.; Balsara, N. P. *Nano Lett.* **2009**, Web publication.
(61) Lascaud, S.; Perrier, M.; Vallee, A.; Besner, S.; Prudhomme, J.; Armand, M. *Macromolecules* **1994**, *27* (25), 7469–7477.
(62) Rosedale, J. H.; Bates, F. S.; Almdal, K.; Mortensen, K.; Wignall, G. D. *Macromolecules* **1995**, *28* (5), 1429–1443.
(63) Blanchard, L.-P.; Hesse, J.; Malhotra, S. L. *Can. J. Chem.* **1974**, *52* (18), 3170–3175.